Received: 26 October 2020 | Revised: 17 December 2020 | Accepted: 18 January 2021

DOI: 10.1111/jmi.13002

Journal of Microscopy RMS

ORIGINAL ARTICLE

Experimental test of the geometric model of image formation in bright-field microscopy

RJ Clements[1] | **M Davidson**[2] | **MA Model**[1]

[1] Department of Biological Sciences, Kent State University, Kent, Ohio

[2] Department of Mathematical Sciences, Kent State University, Kent, Ohio

Correspondence
MA Model, Kent State University, Department of Biological Sciences, Cunningham Hall, Kent, OH 44242.
Email: mmodel@kent.edu

Abstract

In the geometric optics approximation, an image formed by an objective lens replicates the distribution of intensity at the front focal plane of the objective. Although this fact represents a fundamental optical principle, its application to analysis of bright-field microscopic images was developed only recently and has not been tested experimentally. In this paper, we applied simple ray tracing to compute an image of a glass cylinder at various positions of the objective and to compare it to the experiment. We obtained a close match between theory and observation, except for a slight underestimation of the intensity in the middle part of the cylinder. The likely reason for this minor difference was constructive interference due to lens-like properties of a cylinder, which could not be accounted for by geometric approximation. We expect that such artefacts would be negligible in imaging of live cells, and the geometric approach would successfully complement the existing quantitative phase methods.

1 | INTRODUCTION

Quantitative phase imaging (QPI) has developed into a substantial branch of research and industry.[1–3] The immediate output of QPI is the phase delay of light passing through a refractive sample. When the sample is a biological cell, the phase information can be directly related to the mass of the cell's organic matter. When the volume of the cell is known from independent measurements, phase data can be used to calculate the average refractive index and further converted into cell protein and water content.[3,4] In some cases, QPI is used as a cell profiling tool, but that assumes that the refractive index of a cell is known and constant over time and space.

A wide variety of QPI techniques have been developed, most of which are based on optical diffraction theory.[2] But for many applications, such as estimating cell water content, high spatial resolution is inessential, in which case the geometric approximation is justified. One geometric variant of QPI based on the transport-of-intensity (TIE) equation has gained popularity.[5,6]

An equation similar to TIE was derived from geometric optics principles by A. Khitrin (https://physicstoday.scitation.org/do/10.1063/PT.6.4o.20180921a/full/) and colleagues.[7] It is based on the fundamental fact that an image formed by an objective lens replicates the distribution of intensity $I(x, y)$ (real or virtual) at its front focal plane. The focal plane of the objective is conjugate to the plane of the detector and may not coincide with the sample plane if the sample is defocused. A condenser produces a uniform illumination which, in the absence of a sample, translates into a uniform and featureless image. When a refractive sample is present, it changes the direction of light propagation and, consequently, $I(x, y)$. In the limit of small relative refractive indices $n = n_{\text{sample}}/n_{\text{medium}}$ and small relative variations of intensity (which is common in imaging of live biological cells), the intensity is related to the cell's height profile $h(x, y)$ as[7]

$$I^{-1}(x, y) = 1 + \frac{n-1}{2}\nabla^2 h^2(x, y).$$

By using direct ray tracing, the method can be extended to large refraction angles and large differences in refractive indices.

The goal of the present paper was to test the ray tracing approach by applying it to imaging of microscopic glass cylinders. Objects with steep boundaries and large refractive indices are difficult to analyse using conventional techniques, and a good match between theory and observation would validate the theory and open the way to further applications.

2 | METHODS

To simplify the problem, we reduced it to two dimensions by imaging microcylinders in light propagating perpendicular to the axis of the cylinder.

Glass fibre cylindrical spacers, with $n = 1.52$ and nominal diameter 15 μm (Nippon Electric Glass, Schaumburg, IL) were a gift from Douglas Bryant (Kent State University). They were placed on a coverslip and imaged on an IX81 inverted microscope (Olympus) using a 20×/0.7 objective and a condenser at a Kohler position set to NA~0.4. A slit-like aperture (approximately 2 × 16 mm) manufactured at the machine shop of Kent State University was inserted in the front focal plane of the condenser to produce an approximation of two-dimensional illumination. The microcylinder intended for analysis was rotated until its axis was perpendicular to the slit.

The images were recorded with a Sensicam QE camera (PCO AG, Germany) and analysed using ImageJ (https://imagej.nih.gov/ij/).

3 | THEORY

We consider a two-dimensional problem: a disc (which is a cross section of a cylinder) resting on a coverglass and illuminated by in-plane rays coming from the condenser above.

In a wide-field Kohler illumination, every point of an object is illuminated by a cone of light limited by the numerical aperture (NA) of the condenser (Figure 1). We assume that illumination is incoherent, so that the total intensity at every point can be computed as a sum of intensities of individual rays (see Section 6 for justification of this assumption).

According to the geometric model, image brightness at the observation point F (Figure 2) is determined by the intensity of all rays, real and virtual, passing through this point (or more precisely, through a small area around that point).

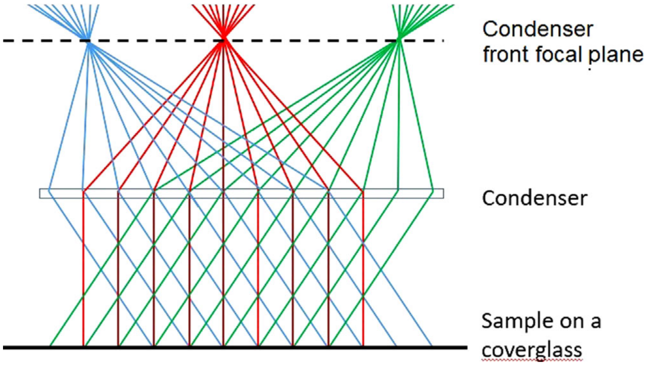

FIGURE 1 Ray diagram of illumination in a wide-field transmission microscope. The light source (a halogen lamp) is focused on the front focal plane of the condenser, producing bundles of collimated rays in the sample space. Inclination angles are limited by the numerical aperture of the condenser NA_{cond}

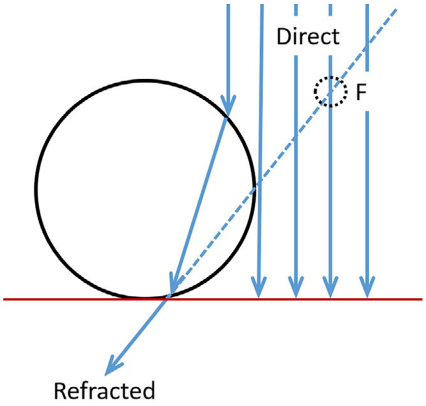

FIGURE 2 The intensity at a circled observation area is the sum of all the refracted rays whose virtual extensions pass through the area and direct illumination where it is unobscured by the disc. Direct illumination is shown for simplicity by vertical lines, but it would be more correctly shown as cones, as in Figure 1

The rays arriving at F have two primary origins. First, there are refracted rays that strike the disc and undergo double refraction on its boundaries (refraction on the coverglass can be disregarded, as it constitutes the normal path of light travel in a microscope and the direction of the ray is restored at the opposite side of the glass). The twice-refracted rays intersect the observation point either directly (if the latter is located in the space between the disc and the coverglass) or as their backward continuation (virtual rays). Second, there is direct illumination I_{dir} coming from the condenser; the disc may fully or partially block it either from the condenser or from the objective. The total intensity I_t is calculated as the sum of direct and refracted intensities:

$$I_t = I_{ref} + I_{dir}. \tag{1}$$

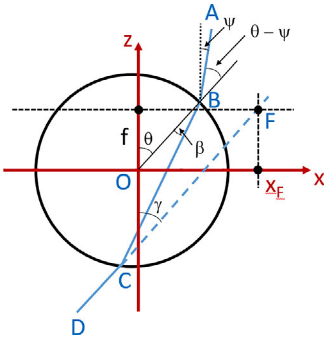

FIGURE 3 Refraction on a disc. An incident ray AB (propagating from the condenser at an angle ψ to the vertical axis z) strikes the disc at point B whose position can be defined by angle θ. The ray undergoes the first refraction into the path BC and the second refraction into CD; CD makes an angle γ with the vertical axis. The objective is focused on the plane $z = f$ (which can be positive or negative). The continuation of the ray CD crosses the plane $z = f$ at point F ($x = x_F$)

In principle, reflected intensity should also be added to Equation (1), but its intensity is low, and we are going to omit it (see Section 6).

The refracted intensity can be calculated as follows. Consider a point B on the surface of a disc with relative refractive index n and radius R; position B can be characterised by the angle θ that the radius OB makes with the vertical axis z (Figure 3). The ray AB propagating from the condenser at an angle ψ with the vertical ($|\psi| < \arcsin \mathrm{NA}_{\mathrm{cond}}$) refracts into the path BC at an angle β to the normal, which is found from Snell's law:

$$\sin\beta = \frac{\sin(\theta - \psi)}{n}. \tag{2}$$

After a second refraction at point C, the ray emerges as CD at an angle

$$\gamma = 2\theta - \psi - 2\beta \tag{3}$$

(see Supplement). If γ lies within the acceptance aperture of the objective $\mathrm{NA}_{\mathrm{obj}}$, it will contribute to the brightness of the image.

Suppose the objective (not shown in the figure) is focused on the plane $z = f$, which can be positive (above the centre of the disc) or negative (below the centre). The ray CD or its continuation backwards crosses the plane $z = f$ at position x_F, which is found by solving the triangles (see Supplement):

$$x_F = [f + \cos(\theta - 2\beta)]\tan(2\theta - \psi - 2\beta) - \sin(\theta - 2\beta). \tag{4}$$

All the distances (x_F and f) are normalised to R. Refracted intensity I_{ref} at x_f is found by summation of the rays for all the θ and ψ that satisfy Equation (4). Points on the disc that are facing the incoming rays more directly (ie at small θ) are exposed to a higher ray density than points on steeper areas (θ approaching 90°), but that factor is automatically included in the computation (see below).

The direct intensity is calculated from Table 1 (see Supplement for the derivation), where

$$q_1 = \arcsin\frac{1}{\sqrt{f^2 + {x_F}^2}} - \arctan\frac{x_F}{f}, \tag{5}$$

$$q_2 = \arcsin\frac{1}{\sqrt{f^2 + {x_F}^2}} + \arctan\frac{x_F}{f}.$$

4 | METHOD OF COMPUTATION

The intensity at a given x_F was represented by the number of rays crossing the interval $\Delta x_F = 0.01$ around each x_F between −3 and 3. The range within $\mathrm{NA}_{\mathrm{cond}}$ ($-0.4 < \psi < \mathrm{NA}$) was divided into $m = 800$ evenly spaced discrete angles ($\Delta\psi = 0.001$) (Figure 4). We also assumed that within each parallel bundle (ie a group of rays propagating at a given ψ) the rays are separated by a lateral distance $w = 0.001$, small compared to the disc radius. Thus, in the absence of any obstacles, a unit length Δx_F receives $m\Delta x_F/w = 8000$ rays (the factor $\cos\psi$ was disregarded since it is small for angles below $\mathrm{NA}_{\mathrm{cond}} = 0.4$, and the true angular distribution of the intensity produced by the condenser is usually not known).

The rays spreading at an angle ψ cross the disc between $\theta_{\min} = \psi - \pi/2$ and $\theta_{\max} = \psi + \pi/2$; thus, one ray was always

TABLE 1 Formulas for I_{dir} expressed as a fraction P of unattenuated intensity. Blank cells indicate that the corresponding relationships are impossible

	$q_1 < -\mathrm{NA}$	$-\mathrm{NA} < q_1 < 0$	$0 < q_1 < \mathrm{NA}$	$q_1 > \mathrm{NA}$
$q_2 < -\mathrm{NA}$	–	–	–	1
$-\mathrm{NA} < q_2 < 0$	–	–	$1 - (q_1 + q_2)/2\mathrm{NA}_{\mathrm{cond}}$	$0.5 - q_2/2\mathrm{NA}$
$0 < q_2 < \mathrm{NA}$	–	$1 - (q_1 + q_2)/2\mathrm{NA}_{\mathrm{cond}}$	$1 - (q_1 + q_2)/2\mathrm{NA}_{\mathrm{cond}}$	$0.5 - q_2/2\mathrm{NA}$
$q_2 > \mathrm{NA}$	1	$0.5 - q_1/2\mathrm{NA}$	$0.5 - q_1/2\mathrm{NA}$	0

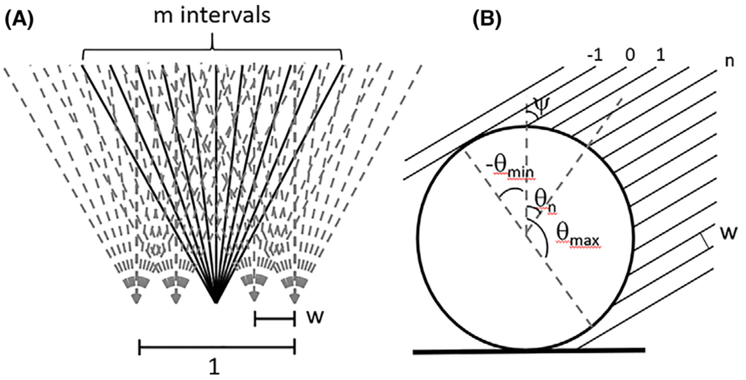

FIGURE 4 Explanation of the parameters used in the computation. (A) Separate points on the sample plane are shown, separated by distance w. Each point is illuminated by an identical cone of light converging from the condenser (see Figure 1) and containing m rays. (B) A group of rays propagating at the same angle ψ (see Figure 3) and crossing the disc at different angles θ. It is assumed that ψ is small enough (eg less than 0.4), so that $\cos\psi \approx 1$, and the lateral separation between oblique rays is close to w

fixed at $\theta_0 = 0$, and all other angles within the above interval were determined by the condition of constant distance w between adjacent rays, resulting in

$$\theta_n = \psi - \arcsin(\sin\psi - wn) \tag{6}$$

(see Supplement). The computation of x_F was performed for every θ_n within the range $(\psi - \pi/2, \psi + \pi/2)$ and every ψ within the range $(-0.4, 0.4)$ provided that $-0.7 < \gamma < 0.7$.

The direct intensity I_{dir} was found as

$$I_{dir} = P\frac{m\Delta x}{w}, \tag{7}$$

where P represents the shading factor due to the disc (Table 1).

The outcome of the computation was a list of x_F for multiple rays. The total number of direct and refracted rays (Equation 1) hitting each subinterval of length Δx was normalised to $m\Delta x/w$.

5 | RESULTS

Images of a microcylinder collected at different positions of the objective are displayed in Figure 5. The zero position was identified by disappearance of small specks on the top surface of the coverslip. Each next image was collected by shifting the objective upward by 2.5 μm. As the objective focal plane keeps shifting upward, the bright centre and dark side shadows (‘Becke lines’) give way to dark centre and bright periphery.

The vertical and lateral distances were recalculated assuming a cylinder diameter of 15 μm and plotted in Figure 6 as orange lines. The corresponding theoretical profiles are shown in blue. In all cases except for $f = -1$, there was a good match between theory and experiment; the experimental intensities are only slightly higher in the middle part of the cylinder.

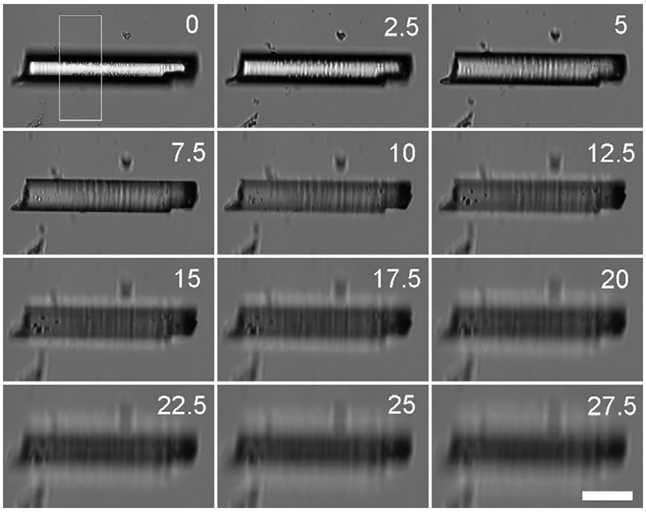

FIGURE 5 Images of a microcylinder collected with a 25×/0.7 objective. The vertical positions in μm relative to the top of a coverslip are shown for each image. The intensity profile was determined as the averaged intensity distribution along the rectangle (shown in the first image). The length of the scale bar is 25 μm

6 | DISCUSSION

The geometric ray tracing method is based on the premise that illumination is incoherent and that interference effects are absent from the image. In reality, transmitted illumination is only partly coherent, and the degree of coherence depends on NA_{cond}: smaller condenser openings produce more coherent light.[8] The geometry of the object also plays a role, and highly symmetrical objects, such as cylinders, are more likely to produce interference artefacts. It is possible that the consistent underestimation of intensity in the central parts of the disc, which was particularly prominent at $f = -1$, was due to constructive interference that was not accounted for by the ray model.

When we attempted to image the same objects in a more closely matched medium ($n = 1.40$), interference lines

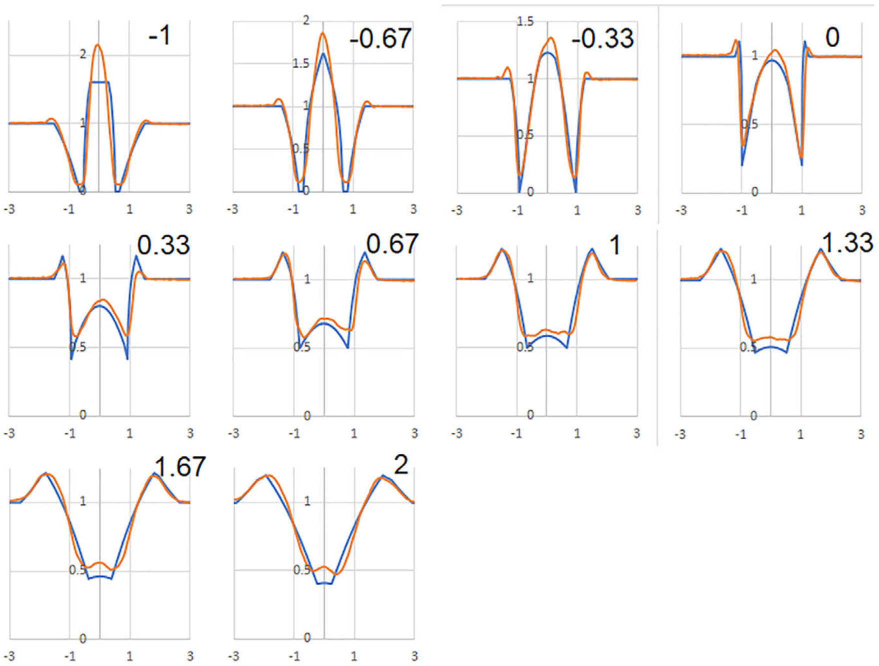

FIGURE 6 Intensity profiles across the cylinder normalised to the background. The experimental values are shown in orange and the calculated values in blue. The horizontal distances and the vertical positions of focal planes (the numbers in the upper right corners) are given in units of the cylinder radius, which was assumed to be 7.5 μm. The lowest position $f = -1$ corresponds to 0 μm in Figure 5 and the highest position at $f = 2$ corresponds to 22.5 μm. The dark and light fringes in Figure 5 correspond, respectively, to the peaks and dips in the intensity profiles

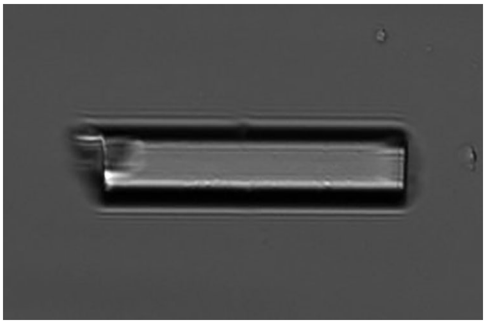

FIGURE 7 Interference lines along the edges of a cylinder immersed in an oil with refractive index 1.4

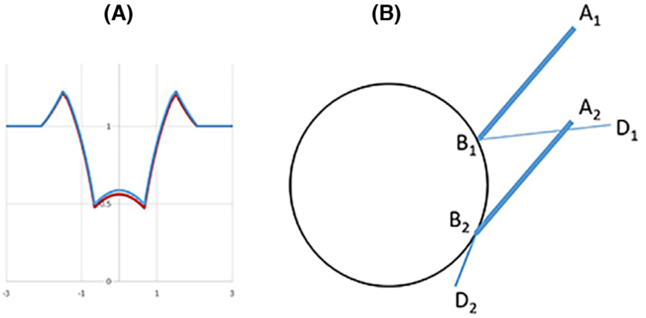

FIGURE 8 The effect of reflection on the intensity distribution. (A) Intensity loss from reflection. The intensity was computed at $f = 1$ without considering reflection (blue line) and with reflection losses included (red line). (B) Intensity gain from reflection. Most reflected rays have low intensity and miss the objective aperture (such as B_1D_1), and only a stronger reflection at extremely oblique angles (B_2D_2) will contribute to the intensity at intermediate values of x. This factor has not been quantitatively evaluated

along the edges were apparent (Figure 7), and such images were unsuitable for analysis.

The other simplification introduced in the model was to disregard reflection. Attenuation of intensity due to reflection losses was computed by introducing Fresnel equations into the code; its effect was mostly a slight (by ~4%) decrease of intensity at small x (Figure 8A). Likewise, we did not include the contribution of reflected rays to the image. Most of them are reflected away from the objective, and the only expected effect would be a small increase in intensity at intermediate x (Figure 8B).

Computing an image of an object with steep boundaries and a high refractive index would be complicated if the wave theory was used. However, the ray tracing approach produced an overall good match between the theory and experiment.

At this stage, it would be premature to claim any specific advantages of the geometric method, other than it is novel and is based on a simple and intuitive principle. To demonstrate its validity, we applied it to a challenging but artificial object, while applications for biological cells still must be developed. The experience shows that cells at moderate resolution can be reasonably well described by geometric models (such as the transport-of-intensity equation) and should be amenable to ray tracing analysis as well.

ORCID

MA Model https://orcid.org/0000-0002-3292-3382

REFERENCES

1. Lee, K., Kim, K., Jung, J., Heo, J., Cho, S., Lee, S., … Park, Y. (2013). Quantitative phase imaging techniques for the study of cell pathopysiology: From principles to applications. *Sensors (Basel)*, *13*(4), 4170–4191. https://doi.org/10.3390/s130404170.
2. Popescu, G. (2011). *Quantitative phase imaging of cells and tissues*. New York: McGraw Hill.
3. Model, M. A., & Petruccelli, J. C. (2018). Intracellular macromolecules in cell volume control and methods of their quantification. *Current Topics in Membranes*, *81*, 237–289.
4. Mudrak, N. J., Rana, P. S., & Model, M. A. (2018). Calibrated brightfield-based imaging for measuring intracellular protein concentration. *Cytometry Part A*, *93*, 297–304.
5. Barty, A., Nugent, K. A., Paganin, D., & Roberts, A. (1998). Quantitative optical phase microscopy. *Optics Letters*, *23*, 817–819.
6. Zuo, C., Li, J., Sun, J., Fan, Y., Zhang, J., Lu, L., … Chen, Q. (2020). Transport of intensity equation: A tutorial. *Optics and Lasers in Engineering*, *22*, 106187.
7. Khitrin, A. K., Petruccelli, J. C., & Model, M. A. (2017). Bright-field microscopy of transparent objects: A ray tracing approach. *Microscopy and Microanalysis*, *23*, 1116–1120.
8. Hopkins, H. H., & Barham, P. M. (1950). The influence of the condenser on microscopic resolution. *Proceedings of the Physical Society, Section B*, *63*, 737–744

SUPPORTING INFORMATION

Additional supporting information may be found online in the Supporting Information section at the end of the article.

How to cite this article: Clements R, Davidson M, Model M. Experimental test of the geometric model of image formation in bright-field microscopy. *Journal of Microscopy*. 2021;*283*:3–8. https://doi.org/10.1111/jmi.13002